THE JOURNAL OF PHYSICAL CHEMISTRY C

Article

pubs.acs.org/JPCC

Tunable Substrate Wettability by Thin Water Layer

Felipe Jiménez-Ángeles[†] and Abbas Firoozabadi[*,†,‡]

[†]Reservoir Engineering Research Institute, Palo Alto, California 94301, United States

[‡]Department of Chemical and Environmental Engineering, Yale University, New Haven, Connecticut 06510, United States

Supporting Information

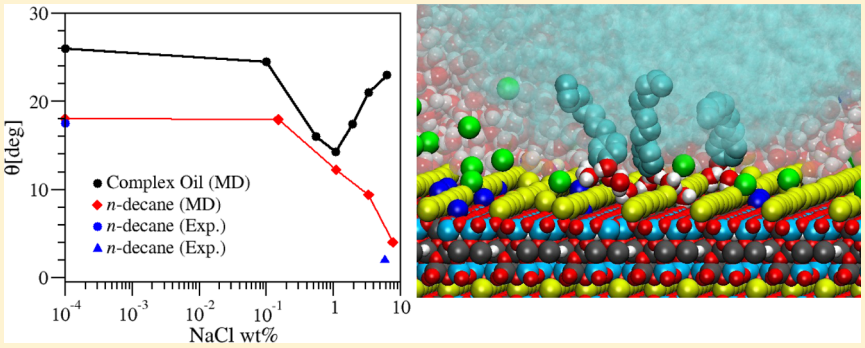

ABSTRACT: In oil−water−mineral substrate systems, we show that the contact angle can be tuned by ionic structures in the water layer confined between an oil droplet and the substrate. We perform molecular dynamics simulations of a complex oil droplet in a NaCl aqueous solution on a mica surface; the oil is a mixture of *n*-decane and surfactant molecules. The surfactant head contains an OH group and an aromatic ring. A thin water layer between the oil droplet and the substrate and ionic stratification regulate the wetting behavior. The concentration of salt ions in the thin film is nonmonotonic; it first increases, then decreases, and starts increasing again as the salt concentration in the bulk increases. On the other hand, the surfactant head adsorption in the thin film first increases as the bulk salt concentration increases. Then, it decreases with further increase in the bulk salt concentration. The change of contact angle with salt concentration also shows a nonmonotonic behavior; the contact angle is first nearly constant to a low salt concentration of 0.1 wt % NaCl. Then, it decreases sharply as the salt concentration increases from 0.1 to 1.1 wt % NaCl. A reverse trend in contact angle follows with further salt concentration increase. The nonmonotonic trend unlike the monotonic trend of interfacial tension with salt concentration is in line with recent measurements of contact angle of oil−brine−substrate systems. A sharp increase of surfactant head adsorption in the thin film, the decrease of ion adsorption, and the minimum of contact angle are all related. This is the first report of such correlations with change of wetting in the brine−complex oil−mineral substrate predicted from molecular simulations.

From living organisms to geological formations, the oil−water−substrate contact is ubiquitous in nature and technology.[1,2] Contact angle can be altered by nanopatterns,[3] nanostructure deposition,[4] electric potentials,[5] and chemical reactions.[6] The oil−water−substrate contact angle is relevant in oil remotion for environmental stewardships,[7−9] metabolism of lipids in living organisms,[10] and hydrocarbon oil recovery[11] among other areas of science and technology. Wettability is defined as the tendency of one fluid to adhere to a solid substrate in the presence of another fluid. Contact angle is a measure of wettability and is related to the two-phase interfacial tensions in Young's equation.[12,13] The macroscopic flow parameters of fluids in porous media, such as capillary pressure and relative permeability, are affected by the fluid−fluid interfacial tensions and contact angle.

In hydrocarbon energy production, injection of seawater (about 4 wt % salt concentration) is used to produce oil from geological formations.[11] In laboratory experiments, it is observed that oil recovery may increase substantially by using low salt concentration solutions.[14−16] Some of the suggested mechanisms of improved oil recovery are based on transition of rock wettability to a state more favorable to oil recovery.[17,18] Recent laboratory measurements show that ions from salt induce wettability changes in oil−water−mineral substrate systems.[19−22] Jones and Ray found that the surface tension of an electrolyte solution shows a minimum at very low salt concentration.[23−27] According to continuous theories and second harmonic generation experiments, the minimum of the electrolyte surface tension is related to a complex balance of the ionic density at the air−water interface.[27−29] In hydrocarbon−electrolyte systems, most of the salts show a monotonic increase of the interfacial tension as a function of the salt concentration;[30,31] some salts may lower the interfacial tension.[30] Contact angle may vary nonmonotonically by salt concentration in a crude oil−aqueous solution−mineral

Received: June 15, 2016
Revised: September 19, 2016
Published: September 19, 2016

DOI: 10.1021/acs.jpcc.6b06054
J. Phys. Chem. C 2016, 120, 24688−24696

substrate system.[22] The microscopic mechanisms of the nonmonotonic wettability by change of the ionic concentration are neither established nor understood and are the subject of this paper.

In molecular simulation studies of a vapor−liquid−substrate, the contact angle variations are due to changes of the fluid−substrate interaction.[32−39] Contact angle changes in liquid−liquid−solid systems have received less attention[40,41] than in vapor−liquid−substrate systems. In a recent molecular dynamics study of a model oil−water−mica system, we observe that the contact angle is regulated by a thin water layer between the oil droplet and the substrate;[42] the contact angle, the water layer thickness, and the ionic adsorption on the substrate follow a monotonic trend as a function of the salt concentration. This work centers on a nonmonotonic trend of contact angle as a function of the salt concentration in a complex oil−water−mica substrate. Our results imply that there is a range of salt concentrations where substrate is in the maximum water wettable state. Our study is carried out by molecular dynamics simulations; our results are in agreement with recent laboratory measurements of the contact angle of petroleum fluids.[22] Additionally, the interfacial tension at the oil−water interface predicted by our model is in agreement with experimental measurements.

MODEL AND SIMULATION METHODS

Fluid−Fluid Interface. First, we simulate the oil−electrolyte solution planar interface as part of this investigation. Two types of oils are studied: (1) simple oil and (2) complex oil. The simple oil is made of 980 *n*-decane molecules, and the complex oil contains 50 surfactant and 980 *n*-decane molecules; the surfactant represents the heteroaromatic oil components.[43] *n*-Decane ($C_{10}H_{22}$) is a 10-bead linear chain modeled by the united atom model potential for alkanes.[44] The surfactant (nonylphenol $C_{15}H_{24}O$) is made of a hexagonal aromatic ring bonded to a nine-carbon linear chain and to an OH group at opposite sides. CH_n (n = 1, 2, 3) groups are modeled as uncharged spherical particles; the oxygen and hydrogen atoms forming the OH group in nonylphenol are represented as two oppositely charged sites; *n*-decane and nonylphenol are shown in Figure 1. Water molecules are represented by the simple charge (SPC) model[45] and simulated as rigid bodies, and Na^+ and Cl^- ions are represented as charged spherical particles using the OPLS force field.[46]

The oil phase is built by placing five *n*-decane layers of 14 × 14 molecules aligned along the z direction in a box of 7 nm × 7 nm × 7 nm. In the complex oil, 25 surfactant molecules are placed at each of the two faces perpendicular to the z direction. The aqueous phase is made of 7625 water molecules, and the number of Na^+ and Cl^- ionic pairs in the solution is $n_+ = n_- =$ 0, 25, 50, 75, 100, and 150 which is equivalent to salt concentrations of 0, 1, 2, 3, 4, and 6 wt %, respectively. The aqueous phase is built in a box of 7 nm × 7 nm × 5 nm. The two fluid boxes are merged to form the fluid−fluid interface.

To equilibrate the system, a 1 ns MD simulation is performed under 3D periodic boundary conditions at T = 293 K and p_z = 1 bar. The pressure and temperature are controlled using the Berendsen barostat and thermostat with relaxation times of τ_T = 0.1 ns and τ_P = 0.4 ns, respectively. A 10 ns run is performed for acquisition of data at T = 293 K and p_z = 1 bar using the Nosé−Hoover[47] thermostat and the Parrinello−Rahman barostat with relaxation times of τ_T = 2 ps and τ_T = 4 ps, respectively. The interfacial tension is computed by[48,49]

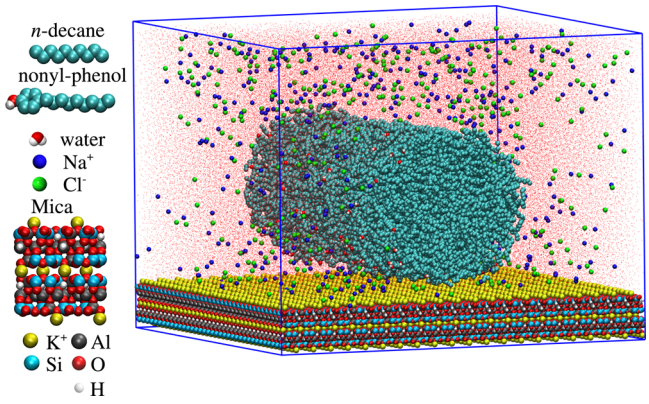

Figure 1. (a) Rotated view of the simulated setup showing water in the bulk solution as red points. (b) Molecular representations: *n*-decane ($C_{10}H_{22}$) is a chain of 10 CH_n beads (cyan); Na^+ and Cl^- ions are spherical particles colored in blue and green, respectively; water is a three-site molecule with oxygen represented in red and hydrogen in white. The components of muscovite mica ($K_2Al_4(Al_2Si_6)O_{20}(OH)_4$) are colored according to the code: Si light blue, Al gray, K yellow, O red, and H white.

$$\gamma = \frac{L_z}{2}\left[p_z - \frac{1}{2}(p_x + p_y)\right] \quad (1)$$

where $p_\alpha = P_{\alpha\alpha}$ with $\alpha = x, y, z$, and the stress tensor is given by

$$P_{\alpha\beta} = \langle \rho_T k_B T \delta_{\alpha\beta} \rangle + \frac{1}{V}\left\langle \sum_i \sum_{j>i} r_{ij}^{\alpha} f_{ij}^{\beta} \right\rangle \quad (2)$$

where r_{ij}^{α} is the α-component of the vector $\mathbf{r}_{ij} = \mathbf{r}_j - \mathbf{r}_i$ and f_{ij}^{β} is the β-component of the vector $\mathbf{f}_{ij} = \mathbf{f}_j - \mathbf{f}_i$; $\mathbf{r}_j$ and $\mathbf{r}_i$ are the positions and $\mathbf{f}_i$ and $\mathbf{f}_j$ are the forces on particles i and j, respectively; ρ_T is the total number density, k_B is the Boltzmann constant, T is the temperature, $\langle ... \rangle$ means the time average, V is the simulation box volume, L_z is the box length along the direction perpendicular to the interface (z), and the summation is carried out over the total number of particles.

Contact Angle. We simulate a complex oil droplet surrounded by an electrolyte solution on a muscovite mica substrate. The complex oil droplet consists of 2340 *n*-decane and 120 nonylphenol molecules. Cylindrical geometry is used[50,51] to remove the line tension effects.[52] The molecular model and the simulated setup are presented in Figure 1. The setup preparation method is explained in Figure S1 of the Supporting Information. The muscovite mica substrate ($K_2Al_4(Al_2Si_6)O_{20}(OH)_4$) is represented by the atomic coordinates and partial charges.[53,54] The molecular structure of muscovite mica is shown in Figure 1. The mica surface charge density of −0.3424 C/m^2 (equivalent to −2.14 e/nm^2; e is the elementary charge) is neutralized by the K^+ ions from the substrate outermost layer (2.14 K^+ ions/nm^2). The substrate atomic layers other than the potassium ions at the outermost layer are kept fixed. The positions of K^+ free ions are nearly unaltered during the simulations due to the strong electrostatic interactions; few K^+ ions are released to the solution in agreement with experimental measurements and previous molecular dynamics simulations.[55] Full replacement of K^+ ions occurs only in the presence of H^+ ions.[56] The composition of the simulated setups is given in Table 1.

DOI: 10.1021/acs.jpcc.6b06054
J. Phys. Chem. C 2016, 120, 24688−24696

Table 1. Simulation Setups

run	N_w	N_d	N_{surf}	$N^+ = N^-$	ρ_s (wt %)
1	108933	2340	120	0	0
2	112262	2340	120	50	0.15
3	114450	2340	120	193	0.55
4	114450	2340	120	393	1.10
5	112235	2340	120	689	1.9
6	112235	2340	120	1189	3.
7	125045	2340	120	2565	6.3

[a] N_w number of water molecules, N_d number of *n*-decane molecules, N_{surf} number of nonylphenol (surfactant) molecules, N^+ and N^- number of sodium and chloride ions, respectively; ρ_s is the salt concentration in weight %.

The simulation box has dimensions of L_x = 18.7 nm and L_y = 18.9 nm in the x and y directions, respectively. The box length in the z direction L_z is adjusted to keep the average pressure at ~200 bar. No significant change of results is observed at a pressure of 100 bar. Periodic boundary conditions are applied in the x and y directions. In the z direction, the simulation box is constrained by a virtual wall at $z = L_z$ by means of a 9-3 Lennard-Jones potential given by[57] $u_{ij}^w(z) = 4\epsilon_w\pi\rho_w\sigma_w^3/3[(\sigma_w/z)^9/15 - (\sigma_w/z)^3/2]$; z is the perpendicular distance to the wall, ρ_w = 20 atoms/nm^3, ϵ_w = 1.3 kJ/mol, and σ_w = 0.37 nm.

Newton's equation of motion is integrated using the leapfrog algorithm. Intermolecular interactions are taken into account through the Lennard-Jones and Coulomb potentials. The Lennard-Jones interactions are truncated at 1.2 nm, and long-range electrostatic interactions are computed using the smooth particle mesh Ewald summation in slab geometry.[58] Bonded neighbor atoms and atomic groups in molecules are kept joined by means of bond constraints at a distance b_0. A harmonic potential around an equilibrium angle θ_0 is used among triplets of neighbor atoms (see the Supporting Information). A torsion potential as a function of the dihedral angle ϕ is used among quadruplets of neighbor atoms (see the Supporting Information). A Berendsen thermostat is used to stabilize temperature during the initial 200 ps of simulations with the parameters τ_T = 0.2 ps followed by an equilibration run using the Nosé–Hoover[47] thermostat with a relaxation time of τ_T = 2 ps. Simulations are conducted in the NVT ensemble at T = 298 K using the open source code Gromacs.[59] No appreciable changes in the shape of the droplet are observed after 28 ns of simulation, which is established as the equilibration criterion. Additional 3 ns (at least) runs are performed to calculate the final average density profiles. The *n*-decane density profile in the y–z plane $\rho_d(y, z)$ is computed using a grid of 200 × 200 nodes. The droplet shape is defined from a contour plot of the density profile of *n*-decane CH_n beads at $\rho_d(y, z) = 0.5\ \rho_b$; ρ_b = 55 mol/L is the average bulk density of *n*-decane beads at the center of the droplet. A circle is fitted to the density contour plot. The contact angle in the aqueous phase is defined by the vertical line passing through the circle center and the straight line from the circle center to the intersection of the circle and the horizontal plane where the droplet profile deviates from circular shape (see the bottom panel of Figure 3a). Our contact angle calculation method is described in the Supporting Information; it is similar to the methods in refs 33 and 50. The density contour plots used to determine the contact angle from our molecular dynamics simulations are provided in the Supporting Information.

RESULTS

Fluid–Fluid Interface. The results for the NaCl brine–*n*-decane interface as well as the NaCl brine–complex oil will be presented here. In the Supporting Information, the interface of KI brine–*n*-decane and KCl brine–*n*-decane will be investigated. The KI brine due to the size of I^- ions results in interfacial tension reduction. Figure 2 shows the results of our study of the fluid–fluid planar interface. Figure 2a depicts the increase of the interfacial tension $(\gamma - \gamma_0)$ in the *n*-decane–electrolyte solution systems as a function of the salt concentration; γ_0 is the salt free and γ is with salt. $(\gamma - \gamma_0)$ increases with salt concentration. The MD simulation results of simple oil are in agreement with the experimental measurements and with previous MD simulations.[30,60] The interfacial tension in the complex oil–electrolyte solution system is lower than that in the simple oil; γ_0 = 49.05 mN/m and γ_0 = 44.05 mN/m in the simple oil and complex oil, respectively. The addition of surfactant lowers the interfacial tension, whereas the addition of salt increases it.

Figure 2b presents the density profiles of the species forming the simple oil–electrolyte solution interface. The origin is set at the middle of the aqueous solution using the 3D periodicity. The hydrocarbon phase is at both sides of the aqueous phase. The water–*n*-decane interfaces are defined by the overlap

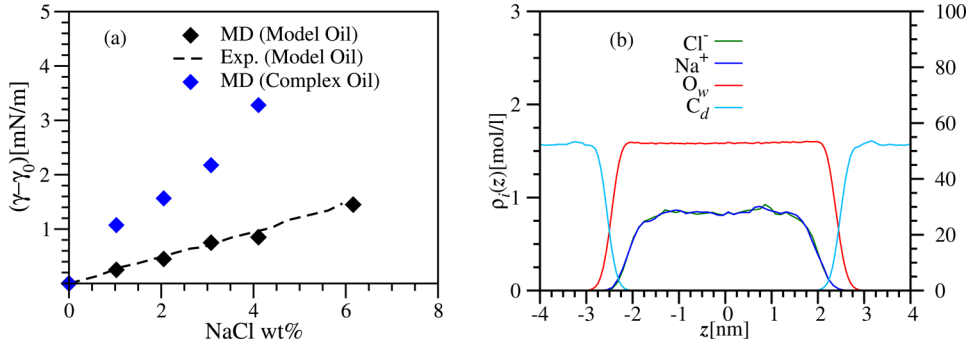

Figure 2. Oil–electrolyte solution planar interface. (a) Interfacial tension increase $(\gamma - \gamma_0)$ as a function of the NaCl concentration in wt % (p_z = 1 bar and T = 293 K). Black and blue diamonds are from MD simulations in simple oil and complex oil, respectively; the dashed line represents the measured interfacial tension in *n*-decane–aqueous phase.[30] The interfacial tensions at zero salt concentration from MD simulations are γ_0 = 49.05 mN/m and γ_0 = 44.05 mN/m in the simple oil and complex oil, respectively; the experimental value in *n*-decane is γ_0 = 52.81 mN/m. (b) Density profiles of Na^+ and Cl^- ions, water-oxygen (O_w), and *n*-decane carbon atoms (C_d) in the simple oil–electrolyte solution interface at ρ_s = 4.2 wt %. The left scale is for the ions, and the right scale is for water-oxygen and *n*-decane.

DOI: 10.1021/acs.jpcc.6b06054
J. Phys. Chem. C 2016, 120, 24688–24696

between the oil and water oxygen density profiles. Away from the interface, the densities are nearly constant. The Na^+ and Cl^- density profiles are overlapped and show that the ions are not found at the interface.

To further validate the predictions of MD simulations, we computed the interfacial tension of the simple oil−electrolyte solution interface of KI and KCl; MD simulation results are in agreement with experimental measurements (see the Supporting Information).

Contact Angle. Our study focuses on the droplet shape and contact angle, the thickness, and structure of the fluid confined between the droplet and the substrate. We first analyze the results from the NaCl salt concentrations ρ_s = 0, 1.1, and 3.4 wt %.

Instantaneous snapshots and complex oil average density contour profiles ($\rho_d(y, z) \approx 0.5\rho_b$) at ρ_s = 0, 1.1, and 3.4 wt % NaCl are shown in parts a, b, and c of Figure 3, respectively.

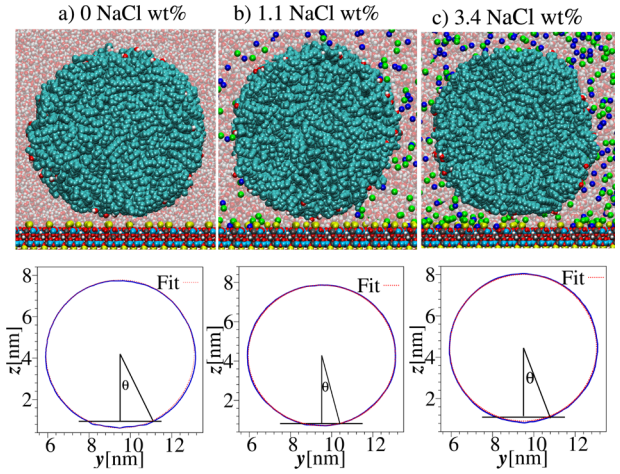

Figure 3. Complex oil droplet in aqueous solutions at (a) ρ_s = 0, (b) ρ_s = 1.1, and (c) ρ_s = 3.4 wt % NaCl; instantaneous droplet snapshot equilibrated by 30 ns molecular dynamics simulations (top) and time averaged contour profile at $\rho_d(y, z) = 0.5\rho_b$ (bottom). Density averaged contour profiles are computed from an additional 4 ns of MD simulations.

The snapshots and the average density contour profiles show that the oil droplets are rugged at the region close to the substrate (bottom) and circular away from the substrate. The droplet rugged section is used to define the contact plane and the contact angle. Different droplet geometries are observed at the three salt concentrations; the contact angles are θ = 26, 14.3, and 21° corresponding to droplet rugged section widths of 3, 1.8, and 2.5 nm at ρ_s = 0, 1.1, and 3.4 wt % NaCl, respectively. The separation distance between the droplet and the substrate is established at equilibrium; the density contour profiles at 0 and 1.1 wt % NaCl are at about the same distance to the substrate, whereas the profile at 3.4 wt % is farther from the substrate.

The oil−water interface close to the substrate at 0 wt % NaCl is analyzed in Figure 4. Figure 4a is a snapshot of a section of the simulation box comprising the bottom part of the droplet, the substrate, and the water liquid layer between the droplet and the substrate. The surfactant molecules (Figure 4a) affect the bottom oil−water interface and the contact angle; they appear mostly aligned upward while their heads are in contact with the aqueous phase. The reduced density profiles of water oxygen atoms, the surfactant head oxygen atoms, and carbon atoms from *n*-decane as a function of the perpendicular distance to the substrate are depicted in Figure 4b. The reduced density profiles (Figure 4b) are computed within the region comprising a droplet horizontal planar section of approximately 3 nm and are normalized with respect to the bulk densities of 53.5 and 55 mol/L for water and *n*-decane, respectively. The reduced density profile of *n*-decane (see Figure 4a) increases from zero in the water layer to a bulk value in the oil droplet. The surfactant head oxygen density profile exhibits an unsymmetrical distribution extending from $z \approx 0.3$ to 1.4 nm and a maximum at $z \approx 0.82$ nm. The density profile of water oxygen (see Figure 4b) shows a sharp peak at $z \approx 0.26$ nm and a small hump at $z \approx 0.20$ nm, indicating the location of the two water layers adsorbed on the substrate. A secondary peak is seen close to the oil phase at $z \approx 0.5$ nm and a hump at $z \approx 0.62$ nm. The peaks may be from shielding the surfactant OH group; we will come back to this point later when we discuss the structure of water around the surfactant head. The water layer thickness δ_e is measured from the sharp peak at $z \approx 0.26$ nm to the point where the reduced density profile is 0.5 at $z \approx 0.76$; it is $\delta_e \approx 0.5$ nm. In Figure 4c, three selected surfactant molecules and the water molecules surrounding the head OH group are shown.

The oil−water interface at the bottom part of the droplet at 1.1 wt % NaCl is examined in Figure 5. Figure 5a shows a snapshot of the water liquid layer between the droplet and the substrate. In the *y* direction, the bottom oil−water interface is

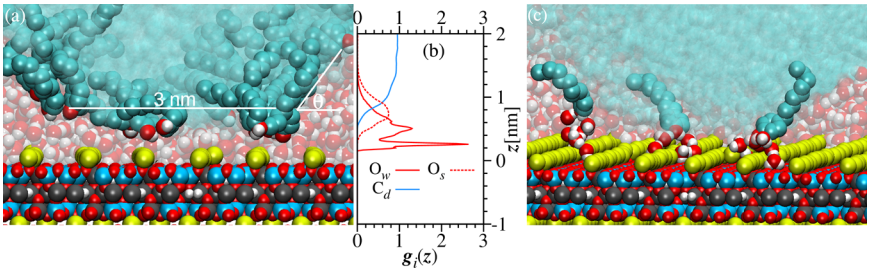

Figure 4. Oil−water layer−substrate at 0 wt % NaCl: (a) Closeup view of the region comprising the bottom part of the droplet, the water liquid layer, and the substrate. The region occupied by *n*-decane molecules is colored transparent-cyan, whereas water molecules are semitransparent and in the background; the color code is the same as that in Figure 1. (b) Reduced density profiles of water oxygen atoms (O_w), *n*-decane carbon atoms (C_d), and the surfactant head oxygen atoms (O_s) in the region between the droplet and the substrate at 0 wt % NaCl. The scales along the *z* direction in parts a and b match. The origin of the perpendicular distance to the substrate is placed above the outermost layer of oxygen atoms from the substrate. (c) Rotated view of the bottom part of the droplet showing three selected surfactant molecules and the water molecules through which they associate with the substrate.

DOI: 10.1021/acs.jpcc.6b06054
J. Phys. Chem. C 2016, 120, 24688−24696

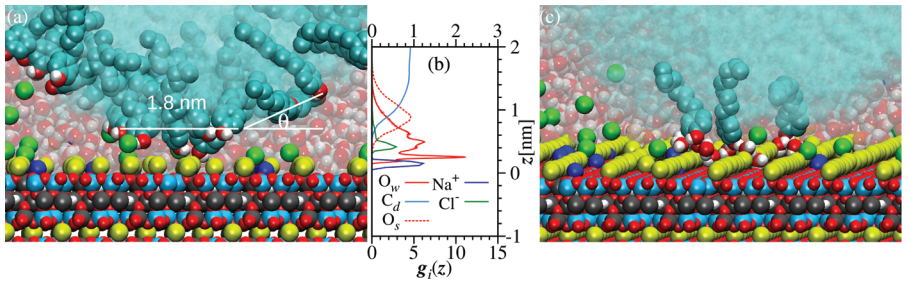

Figure 5. Oil−water layer−substrate at 1.1 wt % NaCl: (a) Closeup view of the region comprising the bottom part of the droplet, the water liquid layer, and the substrate. The region occupied by *n*-decane molecules is colored transparent-cyan, whereas water molecules are semitransparent and in the background; the color code is the same as that in Figure 1. (b) Reduced density profiles of Na^+ and Cl^- ions, water oxygen atoms (O_w), *n*-decane carbon atoms (C_d), and the surfactant head oxygen atoms (O_s) in the region between the droplet and the substrate at 1.1 wt % NaCl. The horizontal scale at the top is for water-oxygen, surfactant oxygen, and *n*-decane; the scale at the bottom is for the ions. The scales along the *z* direction in parts a and b match. The origin of the perpendicular distance to the substrate is placed above the outermost layer of oxygen atoms from the substrate. (c) Rotated view of of the region under the droplet showing three selected surfactant molecules and the water molecules through which they associate with the substrate.

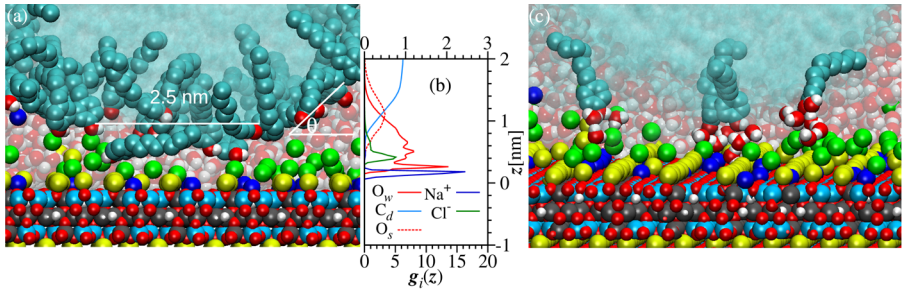

Figure 6. Oil−water layer−substrate at 3.4 wt % NaCl: (a) Closeup view of the region comprising the bottom part of the droplet, the water liquid layer, and the substrate. The region occupied by *n*-decane molecules is colored transparent-cyan, whereas water molecules are semitransparent and in the background; the color code is the same as that in Figure 1. (b) Reduced density profiles of Na^+ and Cl^- ions, water oxygen atoms (O_w), *n*-decane carbon atoms (C_d), and the surfactant head oxygen atoms (O_s) in the region between the droplet and the substrate at 3.4 wt % NaCl. The horizontal scale at the top is for water-oxygen, surfactant oxygen, and *n*-decane; the scale at the bottom is for the ions. The scales along the *z* direction in parts a and b match. The origin of the perpendicular distance to the substrate is placed above the outermost layer of oxygen atoms from the substrate. (c) Rotated view of the region under the droplet showing three selected surfactant molecules and the water molecules through which they associate with the substrate.

narrower at 1.1 wt % NaCl (<2 nm) than in pure water (~3 nm at 0 wt % NaCl), whereas the water layer thickness is similar at both salt concentrations ($\delta_e \approx 0.5$ nm). Due to the strong electrostatic interactions, K^+ ions stay nearly at their initial positions, forming aligned rows even though they are free to move. Away from the droplet, Na^+ and Cl^- ions stratify into two layers; Na^+ ions adsorb on the outermost oxygen atoms of mica next to K^+, while Cl^- ions form a secondary layer above the cations (Na^+ and K^+) layer. The middle region under the droplet is nearly depleted from Na^+ and Cl^- ions; these ions are only found close to the lateral entries of the liquid layer.

Figure 5b portrays the reduced density profiles of Na^+ and Cl^- ions, the water oxygen atoms (O_w), the surfactant head oxygen atoms (O_s), and the carbon atoms from *n*-decane (C_d) as a function of the perpendicular distance to the substrate at the oil−water bottom interface. The reduced density profile of *n*-decane increases monotonically from zero in the water layer to a bulk value inside the oil droplet. The reduced density profile of the water oxygen is similar to that at 0 wt % NaCl; it has a sharp peak at $z \approx 0.26$ nm, a hump at $z \approx 0.20$ nm, and a secondary peak at $z \approx 0.5$. Similarly to the 0% NaCl, the surfactant heads are found between $z \approx 0.3$ and 1.5 nm and are nearly symmetrically distributed around the maximum located at $z \approx 0.82$ nm.

The reduced density profile of Na^+ has a sharp peak at $z \approx 0.1$ nm, whereas the Cl^- density profile has a peak at $z \approx 0.45$ (see Figure 5b). Integration of density profile peaks gives 0.031 Na^+ and 0.025 Cl^- ions/nm^2 adsorbed in the water layer under the droplet. These values reflect the ionic depletion mentioned above. Away from the droplet, there are 0.4 Na^+ ions/nm^2 adsorbed on the substrate and the Cl^- ions are distributed in a diffuse layer. Ionic depletion occurs during the droplet equilibration; at the start of our simulation, it is placed at a separation distance of 0.9 nm from the substrate and a uniform distribution of Na^+ and Cl^- on the whole substrate is observed from the pre-equilibration runs. Despite strong affinity by the substrate, some Na^+ and Cl^- ions are displaced by the oil droplet from the liquid layer region under the droplet. At 0 and 1.1 wt % NaCl, the water layer thickness is $\delta_e \approx 0.5$ nm and the surfactant head distribution is centered at $z \approx 0.8$ nm.

Figure 5c portrays a rotated view of the region under the droplet (1.8 nm width in the *y* direction). Three selected surfactant molecules are shown with the water molecules through which the surfactant head associate with the substrate. The substrate−surfactant association is mediated through hydrogen bonded water. In the thin water layer, the surfactant OH group and the Cl^- ions are found separated by water molecules; a typical Cl^-−OH separation distance is about 0.5 nm. We will come back to this point below when we discuss the

DOI: 10.1021/acs.jpcc.6b06054
J. Phys. Chem. C 2016, 120, 24688−24696

surfactant OH−Cl^- interaction. Because the water layer thickness (z direction) is about 0.5 nm, this separation distance occurs only in the x and y directions. The Cl^-−OH association in the z direction would imply the unfavorable release of intermediate water molecules. The surfactant molecules associate to the substrate without intermediate Cl^- ions (see Figure 5c). The surfactant heads and Cl^- ions compete for the space close to the substrate. At 1.1 wt % NaCl, the competition is balanced by reducing the droplet−substrate contact area and the ionic adsorption in the confined region under the droplet. The result is a reduction of the oil contact angle.

The liquid layer between the droplet and the substrate at 3.4 wt % NaCl is examined in Figure 6. Figure 6a shows a snapshot of a section of the simulation box at the bottom region of the droplet at equilibrium; the water layer thickness of 0.76 nm and the lower planar oil−water interface width is about 2.5 nm. At 3.4 wt % NaCl, ions are found distributed within the whole confined water layer. Na^+ ions adsorb on the substrate outermost oxygen atoms close to the K^+ ion rows, whereas Cl^- ions form a secondary layer above Na^+ and K^+ ions.

Figure 6b presents the reduced density profiles, as a function of the perpendicular distance to the substrate, of Na^+ and Cl^- ions, the water oxygen atoms (O_w), the surfactant head oxygen atoms (O_s), and the carbon atoms from n-decane (C_d). For the reduced density profiles of water oxygen, the hump at $z \approx 0.20$ nm, the sharp peak at $z \approx 0.26$ nm, and the secondary peak at $z \approx 0.5$ nm are common at all of the salt concentrations. The half bulk density value of O_w is at $z \approx 1.02$ nm, giving a water layer thickness of $\delta_e = 0.76$ nm. The ion density profiles are normalized to a bulk number density of 0.6 mol/L. The reduced density profile of Na^+ has a sharp peak at $z \approx 0.2$ nm and a small peak at $z \approx 0.42$ nm. The Cl^- reduced density profile shows a peak at $z \approx 0.4$ nm and decreases to zero toward the oil droplet. The number of ions in the water layer is significantly higher at 3.4 wt % NaCl (0.4 Na^+ and 0.27 Cl^- ions/nm^2) than at 1.1 wt % NaCl (0.031 Na^+ and 0.025 Cl^- ions/nm^2). A larger number of ions in the water layer contribute to a thicker water layer; Cl^- ions are shielded by 7.3 water molecules, whereas Na^+ ions adsorbed to the substrate have between 2 and 3 water molecules in their hydration layer. The reduced density profile of n-decane in Figure 6b is shifted upward compared to the profile in Figure 5b as a consequence of the thicker water layer at higher NaCl concentration. The surfactant heads are found between $z \approx 0.4$ and 1.8 nm, and the maximum of the distribution is located at $z \approx 1$ nm.

Figure 6c is a rotated view of the region under the droplet and shows surfactant molecules shielded by intermediate hydrogen bonded water. Surfactant molecules are adsorbed above the Cl^- secondary layer (see the molecules at the left and right sides). The association between the Cl^- ions and the surfactant head is carried out through intermediate water molecules; the surfactant OH group may form hydrogen bonds with water molecules around the Cl^- ions. The 0.76 nm thick water layer allows the association between OH groups and Cl^- ions in the z direction.

The interaction between the surfactant head and the thin liquid layer is analyzed by means of the radial distribution functions with respect to the surfactant oxygen atom. The calculation (presented in Figure 7) is based on 10 surfactant molecules located at the droplet bottom region in an interval of 1 ns. The radial distribution functions $g(r)$ of the water oxygen (O_w), water hydrogen (H_w), and Na^+ and Cl^- ions at 0.5, 1.1, and 3.3 wt % NaCl are presented in parts a, b, and c of Figure 7, respectively. The positions of the water peaks are the same at the three concentrations; for oxygen, there is a peak at $r \approx 0.28$ nm and there are two peaks for hydrogen at $r \approx 0.18$ and $r \approx 0.31$ nm. The Na^+ radial distribution functions have no peaks, indicating a negligible Na^+−OH association. The Cl^- radial distribution function at 0.5 wt % NaCl has a small peak at $r \approx 0.5$ nm, at 1.1 wt % NaCl it has a maximum at $r \approx 0.5$ nm, and at 3.3 wt % NaCl it has a sharp peak at $r \approx 0.31$ nm and a broader peak at $r \approx 0.75$ nm. The positions of the main peaks imply that the surfactant head oxygen atom is surrounded by water molecules. The Cl^- sharp peak at 3.3 wt % NaCl indicates an association between the surfactant OH group and Cl^- mediated by water molecules. This association likely contributes to the droplet spreading on the ions at the 3.3 wt % NaCl as we mentioned in the discussion of Figure 6.

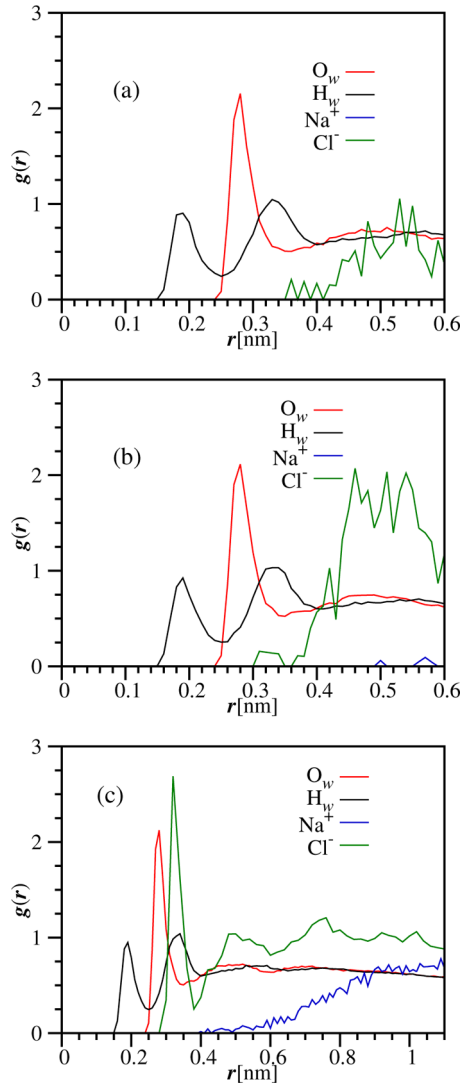

Figure 7. Radial distribution function of oxygen water (O_w) and Na^+ and Cl^- ions with respect to the surfactant head oxygen at (a) 0.5, (b) 1.1, and (c) 3.3 wt % NaCl.

The contact angles θ from MD simulations as a function of the salt concentration for the model n-decane oil and complex oil are plotted in Figure 8a. A monotonically decreasing trend is observed in the contact angle of the n-decane model oil.[42] The complex oil shows a nonmonotonic behavior as a function of

DOI: 10.1021/acs.jpcc.6b06054
J. Phys. Chem. C 2016, 120, 24688−24696

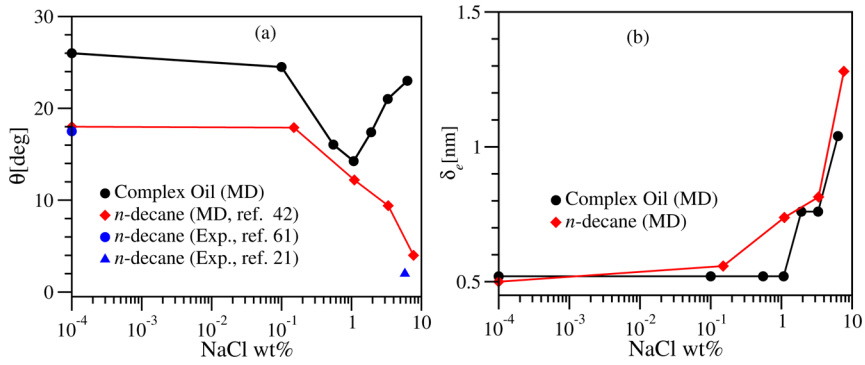

Figure 8. (a) Contact angle θ of complex oil as a function of salt concentration in the aqueous phase; measurements and molecular dynamics simulations for *n*-decane are included from refs 21, 42, and 61. (b) Confined water layer thickness under the complex oil droplet (black bullets) and *n*-decane droplet (diamonds) as a function of salt concentration. Straight lines join points to guide the view.

the salt concentration; the contact angle is about 25° in the range from 0 to 0.15 wt % NaCl, from 0.03 to 1 wt % NaCl it decreases to 14.3°, and then it increases to $\theta \approx 24°$ at 6.3 wt % NaCl. The nonmonotonic behavior and the location of the minimum are in agreement with recent measurements in a crude oil−brine−mica system.[22] The water layer thickness δ_e as a function of the salt concentration is portrayed in Figure 8b. The water layer thickness of the *n*-decane model oil[42] increases monotonically from $\delta_e \approx 0.5$ nm at 0 wt % NaCl to $\delta_e \approx 1.3$ nm at wt % 7.7 NaCl. For the complex oil, the water layer thickness remains constant at $\delta_e = 0.5$ nm from 0 to 1.1 wt % NaCl; a steep increase is seen to about 1.1 nm at 6.6 wt % NaCl.

The adsorption of species *i* is defined as

$$\Gamma_i = \int_0^{z_1} \rho_i(z)\, dz \tag{3}$$

where $\rho_i(z)$ is the density profile of species *i* within the fluid region confined between the substrate and the oil phase and z_1 is a distance along the *z* direction comprising the adsorbed molecules in the confined region.

The adsorption of the surfactant head and the Na^+ and Cl^- ions in the confined region under the droplet is examined in parts a, b, and c of Figure 9, respectively. The density profile of the surfactant head oxygen (O_s) is used to compute the surfactant head adsorption. The three species (surfactant, Na^+, and Cl^-) exhibit a nonmonotonic behavior as a function of the bulk salt concentration. The surfactant adsorption has a maximum at $\rho_s = 1.1$ NaCl wt %, and then, it decreases. The adsorption of the Na^+ and Cl^- ion first increases, then decreases at $\rho_s = 1.1$ NaCl wt %, and then increases again at higher salt concentration. The adsorption of Na^+ and Cl^- ions under a droplet of simple oil (without surfactant, Figure 9b and c) increases monotonically as a function of the bulk salt concentration. The nonmonotonic adsorption is also observed in the reduced density profiles in Figure S8 in the Supporting Information. The contact angle in the complex oil shows a nonmonotonic trend similar to the Jones−Ray effect.[23−27]

Wettability alteration in oil−rock systems is often modeled as the interaction between two charged interfaces. The charges at the oil−water interface are attributed to the dissociation of chemical species in the oil. The interaction between two charged interfaces is described by the DLVO theory of the double layer.[11,62,63] According to that theory, the equilibrium thickness of the water layer increases as the characteristic Debye length increases (κ^{-1}), namely, as the salt concentration decreases. Even though the double layer screening length in our

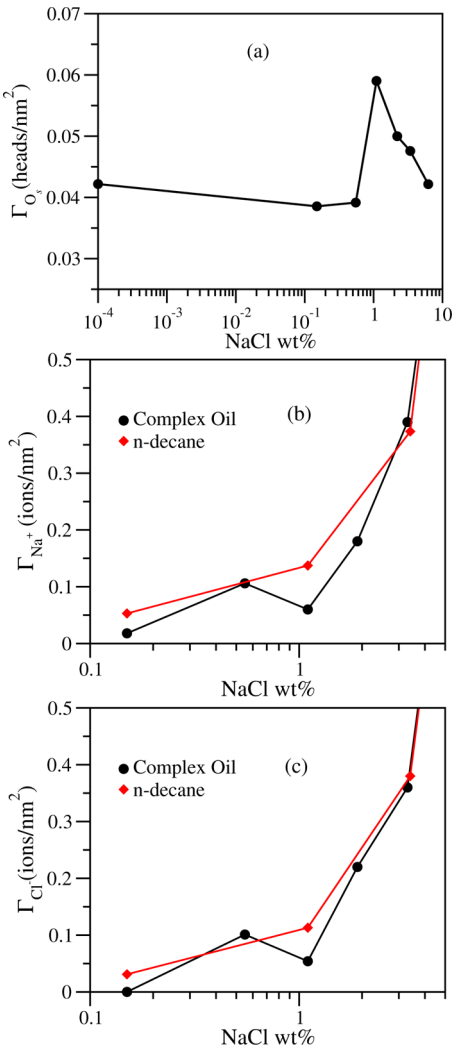

Figure 9. Adsorption as a function of the bulk salt concentration in the confined thin layer: (a) surfactant, (b) Na^+, and (c) Cl^-; bullets represent the results from the complex oil droplet and diamonds from the *n*-decane droplet.

simulations is similar to the Debye length, the DLVO theory is not applicable because the oil phase does not have an effective charge. In our molecular simulation, hydration forces and ionic adsorption play a fundamental role.[64] The oil−substrate association is through hydrogen bonds and the ions provide a

DOI: 10.1021/acs.jpcc.6b06054
J. Phys. Chem. C 2016, 120, 24688−24696

water solvation shell. The disruption of hydrogen bonds has a significant free energy cost. In the low salt concentration regime, the surfactant−substrate association maintains a thin liquid layer at the expense of reducing the contact area and expelling ions from the thin liquid layer. Above a certain salt concentration, the water layer region under the droplet expands and ions penetrate to the thin film. The overall behavior is that the water layer thickness increases in a stepwise manner as the salt concentration increases while the contact angle follows a nonmonotonic trend.

CONCLUSIONS

In our simulations, a thin liquid water layer between the substrate and the oil droplet regulates wettability. Ions are adsorbed to the substrate through electrostatic attraction, whereas the surfactant−substrate association is through hydrogen bonds between the OH-headgroup and intermediate water molecules. Association between the Cl^- ions and the surfactant head OH group is through intermediate water molecules.

In the low salt concentration regime (<1.1 NaCl wt %), we observe the following in the thin water layer: (1) The water layer thickness is constant at about 0.5 nm. (2) Ionic adsorption may decrease as a function of the bulk salt concentration. (3) The Cl^-−OH association along the z direction does not occur due to the small film thickness. (4) As the bulk salt concentration increases, the Cl^- ions occupy a larger area next to the substrate and surfactant is constrained to a smaller area; the result is a reduction of the oil droplet contact angle.

At salt concentrations above 1.1 NaCl wt %, we observe the following in the thin liquid layer: (1) The water layer thickness is $\delta_e > 0.78$ nm, and the oil droplet moves away farther from the substrate. (2) Ionic adsorption increases as a function of the bulk salt concentration. (3) Cl^-−OH association in the z direction occurs due to a thicker water layer. (4) The droplet spreads on the Cl^- ionic layer; the contact angle begins to increase as a function of the salt concentration.

The nonmonotonic contact angle is correlated with the nonmonotonic behavior of the surfactant head and ion adsorption in the confinement and with the step increase of the water layer thickness. In a simple oil without polar molecules, the ionic adsorption and the water layer thickness increase monotonically while the contact angle decreases monotonically as a function of salt concentration. The hydrocarbon−water interfacial tension from our MD is in agreement with experimental measurements. Furthermore, the nonmonotonic behavior of the complex oil droplet contact angle as a function of the bulk salt concentration from our MD simulations is in line with recent measurements in petroleum fluids.[22]

ASSOCIATED CONTENT

Supporting Information

The Supporting Information is available free of charge on the ACS Publications website at DOI: 10.1021/acs.jpcc.6b06054.

Contact angle setup construction, contact angle calculation method, fluid−fluid interface with KCl and KI, thin liquid layer at 0.1, 1.1, and 6.2 NaCl wt %, ionic adsorption as a function of salt concentration, simulation parameters, and references (PDF)

AUTHOR INFORMATION

Corresponding Author

*E-mail: abbas.firoozabadi@yale.edu. Phone: +1 (650)326-9172. Fax: +1 (650) 472-9285.

Notes

The authors declare no competing financial interest.

ACKNOWLEDGMENTS

We thank Chevron Corporation and the member companies of the Reservoir Engineering Research Institute (RERI) for their financial support of this work. We thank Dr. Nariman Fathi Najafabadi of Chevron Corporation for his interest and discussions.

REFERENCES

(1) Kvenvolden, K. A. Organic geochemistry - A retrospective of its first 70 years. *Org. Geochem.* **2006**, *37*, 1−11.
(2) Alberts, B.; Johnson, A.; Lewis, J.; Raff, M.; Roberts, K.; Walter, P. *Molecular Biology of the Cell*; Garland Science: New York, 2002.
(3) Schellenberger, F.; Encinas, N.; Vollmer, D.; Butt, H.-J. How Water Advances on Superhydrophobic Surfaces. *Phys. Rev. Lett.* **2016**, *116*, 096101.
(4) Chen, K.-Y.; Ivashenko, O.; Carroll, G. T.; Robertus, J.; Kistemaker, J. C. M.; London, G.; Browne, W. R.; Rudolf, P.; Feringa, B. L. Control of Surface Wettability Using Tripodal Light-Activated Molecular Motors. *J. Am. Chem. Soc.* **2014**, *136*, 3219−3224.
(5) Mugele, F.; Baret, J. C. Electrowetting: From Basics to Applications. *J. Phys.: Condens. Matter* **2005**, *17*, R705.
(6) Factorovich, M. H.; Molinero, V.; Scherlis, D. A. Hydrogen-Bond Heterogeneity Boosts Hydrophobicity of Solid Interfaces. *J. Am. Chem. Soc.* **2015**, *137*, 10618−10623.
(7) Yuan, J.; Xiaogang, L.; Ozge, A.; Junqing, H.; Steven L, S.; Jing, K.; Francesco, S. Superwetting Nanowire Membranes for Selective Absorption. *Nat. Nanotechnol.* **2008**, *3*, 332−336.
(8) Lahann, J. Environmental Nanotechnology: Nanomaterials Clean Up. *Nat. Nanotechnol.* **2008**, *3*, 320−321.
(9) Lahann, J.; Mitragotri, S.; Tran, T. N.; Kaido, H.; Sundaram, J.; Choi, I. S.; Hoffer, S.; Somorjai, G. A.; Langer, R. A Reversibly Switching Surface. *Science* **2003**, *299*, 371−374.
(10) Stryer, L. *Biochemistry*, 4th ed.; W.H. Freeman and Company: New York, 1995.
(11) Myint, P. C.; Firoozabadi, A. Thin Liquid Films in Improved Oil Recovery from Low-Salinity Brine. *Curr. Opin. Colloid Interface Sci.* **2015**, *20*, 105−114.
(12) Israelachvilli, J. N. *Intermolecular and Surface*, 3rd ed.; Academic Press: London, 1992.
(13) de Gennes, P. G. Wetting: Statics and Dynamics. *Rev. Mod. Phys.* **1985**, *57*, 827−863.
(14) Tang, G. Q.; Morrow, N. R. Influence of Brine Composition and Fines Migration on Crude Oil/Brine/Rock Interactions and Oil Recovery. *J. Pet. Sci. Eng.* **1999**, *24*, 99−111.
(15) Zhang, Y.; Xie, X.; Morrow, N. R. Waterflood Performance by Injection of Brine with Different Salinity for Reservoir Cores. *SPE* 2007, *109849*, 1045−1057, 10.2118/109849-MS, SPE Annual Technical Conference and Exhibition, Nov 11−14, Anaheim, CA.
(16) Al-Shalabi, E. W.; Sepehrnoori, K. A Comprehensive Review of Low Salin-ity/Engineered Water Injections and Their Applications in Sandstone and Carbonate Rocks. *J. Pet. Sci. Eng.* **2016**, *139*, 137−161.
(17) Shalabi, E. W. A.; Sepehrnoori, K.; Delshad, M. Mechanisms Behind Low Salinity Water Injection in Carbonate Reservoirs. *Fuel* **2014**, *121*, 11−19.
(18) Sheng, J. Critical Review of Low-Salinity Waterflooding. *J. Pet. Sci. Eng.* **2014**, *120*, 216−224.
(19) Lashkarbolooki, M.; Ayatollahi, S.; Riazi, M. Effect of Salinity, Resin, and Asphaltene on the Surface Properties of Acidic Crude Oil/Smart Water/Rock System. *Energy Fuels* **2014**, *28*, 6820−6829.

DOI: 10.1021/acs.jpcc.6b06054
J. Phys. Chem. C 2016, 120, 24688−24696

(20) Mahani, H.; Keya, A. L.; Berg, S.; Bartels, W.-B.; Nasralla, R.; Rossen, W. R. Insights into the Mechanism of Wettability Alteration by Low-Salinity Flooding (LSF) in Carbonates. *Energy Fuels* **2015**, *29*, 1352−1367.
(21) Mugele, F.; Bera, B.; Cavalli, A.; Siretanu, I.; Maestro, A.; Duits, M.; Cohen-Stuart, M.; van den Ende, D.; Stocker, I.; Collins, I. Ion Adsorption-Induced Wetting Transition in Oil-Water-Mineral Systems. *Sci. Rep.* **2015**, *5*, 10519.
(22) Aslan, S.; Najafabadi, N. F.; Firoozabadi, A. Non-monotonicity of the Contact Angle from NaCl and $MgCl_2$ Concentrations in Two Petroleum Fluids on Atomistically Smooth Surfaces. *Energy Fuels* **2016**, *30*, 2858−2864.
(23) Jones, G.; Ray, W. A. The Surface Tension of Solutions. *J. Am. Chem. Soc.* **1935**, *57*, 957−958.
(24) Jones, G.; Ray, W. A. The Surface Tension of Solutions of Electrolytes as a Function of the Concentration II. *J. Am. Chem. Soc.* **1941**, *63*, 288−294.
(25) Jones, G.; Ray, W. A. The Surface Tension of Solutions of Electrolytes as a Function of the Concentration. III. Sodium Chloride. *J. Am. Chem. Soc.* **1941**, *63*, 3262−3263.
(26) Jones, G.; Ray, W. A. The Surface Tension of Solutions of Electrolytes as a Function of the Concentration. IV. Magnesium Sulfate. *J. Am. Chem. Soc.* **1942**, *64*, 2744−2745.
(27) Petersen, P. B.; Saykally, R. J. Adsorption of Ions to the Surface of Dilute Electrolyte Solutions: The Jones-Ray Effect Revisited. *J. Am. Chem. Soc.* **2005**, *127*, 15446−15452.
(28) Karraker, K.; Radke, C. Disjoining Pressures, Zeta Potentials and Surface Tensions of Aqueous Non-Ionic Surfactant/Electrolyte Solutions: Theory and Comparison to Experiment. *Adv. Colloid Interface Sci.* **2002**, *96*, 231−264.
(29) Manciu, M.; Ruckenstein, E. Specific Ion Effects Via Ion Hydration: I. Surface Tension. *Adv. Colloid Interface Sci.* **2003**, *105*, 63−101.
(30) Aveyard, R.; Saleem, S. M. Interfacial Tensions at Alkane-Aqueous Electrolyte Interfaces. *J. Chem. Soc., Faraday Trans. 1* **1976**, *72*, 1609−1617.
(31) Chávez-Miyauchi, T.; Firoozabadi, A.; Fuller, G. G. Non-Monotonic Elasticity of the Crude Oil-Brine Interface in Relation to Improved Oil Recovery. *Langmuir* **2016**, *32*, 2192−2198.
(32) Sikkenk, J. H.; Indekeu, J. O.; van Leeuwen, J. M. J.; Vossnack, E. O. Molecular-Dynamics Simulation of Wetting and Drying at Solid-Fluid Interfaces. *Phys. Rev. Lett.* **1987**, *59*, 98−101.
(33) Ingebrigtsen, T.; Toxvaerd, S. Contact Angles of Lennard-Jones Liquids and Droplets on Planar Surfaces. *J. Phys. Chem. C* **2007**, *111*, 8518−8523.
(34) Shi, B.; Dhir, V. K. Molecular Dynamics Simulation of the Contact Angle of Liquids on Solid Surfaces. *J. Chem. Phys.* **2009**, *130*, 034705.
(35) Becker, S.; Urbassek, H. M.; Horsch, M.; Hasse, H. Contact Angle of Sessile Drops in Lennard-Jones Systems. *Langmuir* **2014**, *30*, 13606−13614.
(36) Shih, C.-J.; Wang, Q. H.; Lin, S.; Park, K.-C.; Jin, Z.; Strano, M. S.; Blankschtein, D. Breakdown in the Wetting Transparency of Graphene. *Phys. Rev. Lett.* **2012**, *109*, 176101.
(37) Rafiee, J.; Mi, X.; Gullapalli, H.; Thomas, A. V.; Yavari, F.; Shi, Y.; Ajayan, P. M.; Koratkar, N. A. Wetting Transparency of Graphene. *Nat. Mater.* **2012**, *11*, 217−222.
(38) Shih, C.-J.; Strano, M.-S.; Blankschtein, D. Wetting Translucency of Graphene. *Nat. Mater.* **2013**, *12*, 866−869.
(39) Giovambattista, N.; Debenedetti, P. G.; Rossky, P. J. Effect of Surface Polarity on Water Contact Angle and Interfacial Hydration Structure. *J. Phys. Chem. B* **2007**, *111*, 9581−9587.
(40) Seveno, D.; Blake, T. D.; Goossens, S.; Coninck, J. D. Predicting the Wetting Dynamics of a Two-Liquid System. *Langmuir* **2011**, *27*, 14958−14967.
(41) Kumar, V.; Errington, J. R. Understanding Wetting of Immiscible Liquids Near a Solid Surface Using Molecular Simulation. *J. Chem. Phys.* **2013**, *139*, 064110.
(42) Jiménez-Ángeles, F.; Firoozabadi, A. Contact Angle, Liquid Film, Liquid-Liquid and Liquid-Solid Interfaces in Model Oil-Brine-Substrate Systems. *J. Phys. Chem. C* **2016**, *120*, 11910−19917.
(43) Gough, M. A.; Rowland, S. J. Characterization of Unresolved Complex Mixtures of Hydrocarbons in Petroleum. *Nature* **1990**, *344*, 648−650.
(44) Martin, M. G.; Siepmann, J. I. Transferable Potentials for Phase Equilibria. 1. United-Atom Description of n-Alkanes. *J. Phys. Chem. B* **1998**, *102*, 2569−2577.
(45) Berendsen, H. J. C.; Postma, J. P. M.; van Gunsteren, W. F.; Hermans, J. In *Intermolecular Forces*; Pullman, B., Ed.; Reidel: Dordrecht, The Netherlands, 1981; Chapter Simple Point Charge Water.
(46) Jorgensen, W. L. In *The Encyclopedia of Computational Chemistry*; von Ragué Schleyer, P., Ed.; John Wiley & Sons: Dordrecht, The Netherlands, 1998; Vol. 3; Chapter OPLS Force Fields.
(47) Nosé, S. A. Unified Formulation of the Constant Temperature Molecular-Dynamics Methods. *J. Chem. Phys.* **1984**, *81*, 511−519.
(48) de Miguel, E.; Jackson, G. The Nature of the Calculation of the Pressure in Molecular Simulations of Continuous Models from Volume Perturbations. *J. Chem. Phys.* **2006**, *125*, 164109.
(49) Vega, C.; de Miguel, E. Surface Tension of the most Popular Models of Water by Using the Test-Area Simulation Method. *J. Chem. Phys.* **2007**, *126*, 154707.
(50) Weijs, J. H.; Marchand, A.; Andreotti, B.; Lohse, D.; Snoeijer, J. H. Origin of Line Tension for a Lennard-Jones Nanodroplet. *Phys. Fluids* **2011**, *23*, 022001.
(51) Tenney, C. M.; Cygan, R. T. Molecular Simulation of Carbon Dioxide, Brine, and Clay Mineral Interactions and Determination of Contact Angles. *Environ. Sci. Technol.* **2014**, *48*, 2035−2042.
(52) Firoozabadi, A. *Thermodynamics and Applications in Hydrocarbons Energy Production*; McGraw Hill: New York, 2015.
(53) Heinz, H.; Koerner, H.; Anderson, K. L.; Vaia, R. A.; Farmer, B. L. Force Field for Mica-Type Silicates and Dynamics of Octadecylammonium Chains Grafted to Montmorillonite. *Chem. Mater.* **2005**, *17*, 5658−5669.
(54) Guven, N. The Crystal Structures of 2M1 Phengite and 2M1Muscovite. *Z. Kristallogr. - Cryst. Mater.* **1971**, *134*, 196−212.
(55) Sakuma, H.; Kawamura, K. Structure and Dynamics of Water on Muscovite Mica Surfaces. *Geochim. Cosmochim. Acta* **2009**, *73*, 4100−4110.
(56) Israelachvili, J. N.; Adams, G. E. Measurement of Forces Between Two Mica Surfaces in Aqueous Electrolyte Solutions in the Range 0−100 nm. *J. Chem. Soc., Faraday Trans. 1* **1978**, *74*, 975−1001.
(57) Abraham, F. F.; Singh, Y. The Structure of a Hard-Sphere Fluid in Contact with a Soft Repulsive Wall. *J. Chem. Phys.* **1977**, *67*, 2384−2385.
(58) Yeh, I.-C.; Berkowitz, M. L. Ewald Summation for Systems with Slab Geometry. *J. Chem. Phys.* **1999**, *111*, 3155−3162.
(59) Hess, B.; Kuttner, C.; van der Spoel, D.; Lindahl, E. GROMACS 4: Algorithms for Highly Effcient, Load-Balanced, and Scalable Molecular Simulation. *J. Chem. Theory Comput.* **2008**, *4*, 435−447.
(60) van Buuren, A. R.; Marrink, S. J.; Berendsen, H. J. C. A Molecular Dynamics Study of the Decane/Water Interface. *J. Phys. Chem.* **1993**, *97*, 9206−9212.
(61) Schultz, J.; Tsutsumi, K.; Donnet, J.-B. Surface Properties of High-Energy Solids. *J. Colloid Interface Sci.* **1977**, *59*, 272−276.
(62) Tokunaga, T. K. DLVO-Based Estimates of Adsorbed Water Film Thicknesses in Geologic CO2 Reservoirs. *Langmuir* **2012**, *28*, 8001−8009.
(63) Hassan, M.; Steffen, B.; Denis, I.; Willem-Bart, B.; Vahid, J.-N. Kinetics of Low-Salinity-Flooding Effect. *SPE-165255-PA*.
(64) Chandler, D. Interfaces and the Driving Force of Hydrophobic Assembly. *Nature* **2005**, *437*, 640−647.

DOI: 10.1021/acs.jpcc.6b06054
J. Phys. Chem. C 2016, 120, 24688−24696